Journal of Solid State Chemistry **146,** 137–143 (1999)
Article ID jssc.1999.8319, available online at http://www.idealibrary.com on IDEAL®

Synthesis, Crystal Structure, and Magnetic Properties of New One-Dimensional Oxides Ca_3CoRhO_6 and Ca_3FeRhO_6

Seiji Niitaka,*,[1] Hiroshi Kageyama,† Masaki Kato,* Kazuyoshi Yoshimura,* and Koji Kosuge*

*Division of Chemistry, Graduate School of Science, Kyoto University, Kyoto 606-8502, Japan; and †Institute for Solid State Physics, University of Tokyo, Tokyo 106-8666, Japan

Received November 4, 1998; in revised form March 21, 1999; accepted April 8, 1999

One-dimensional compounds Ca_3CoRhO_6 and Ca_3FeRhO_6 have been newly synthesized and structurally characterized by Rietveld refinement of powder X-ray diffraction data. Both compounds are isostructural with the rhombohedral K_4CdCl_6-type structure (space group $R\bar{3}c$; $Z = 6$; Ca_3CoRhO_6: $a = 9.2017(1)$ Å, $c = 10.7296(1)$ Å; Ca_3FeRhO_6: $a = 9.1960(1)$ Å, $c = 10.7861(1)$ Å). The structure of Ca_3CoRhO_6 and Ca_3FeRhO_6 contains one-dimensional chains consisting of alternating faced-sharing CoO_6, FeO_6 trigonal prisms, and RhO_6 octahedra, respectively. The magnetic susceptibility of Ca_3CoRhO_6 exhibits an abrupt drop at 35 K, which is also observed in Sr_3NiIrO_6 and Ca_3CoIrO_6. Ca_3FeRhO_6 is an antiferromagnet with $T_N = 12$ K. © 1999 Academic Press

Key Words: **new one-dimensional oxide; Ca_3CoRhO_6; Ca_3FeRhO_6.**

1. INTRODUCTION

Low-dimensional materials have attracted many researchers because of their unique electronic and magnetic properties. For example, the physical properties of $CuGeO_3$ (spin-Peierls transition) (1), Y_2BaNiO_5 (Haldane gap) (2), and $CsCoCl_3$ (spin-frustrated system) (3) have been extensively investigated. These interesting physical properties of low-dimensional materials originate from the strong directional interactions between spins.

Since Sr_3CuPtO_6 (4) was discovered to be formed in the K_4CdCl_6-type structure having one-dimensional (1-D) chains, many compounds with the general formula A'_3ABO_6 (A' = Sr, Ca, …; A = Cu, Ni, Co, …; B = Ir, Pt, …) have been synthesized. Figure 1a shows the structure of A'_3ABO_6-type compounds. This structure contains 1-D chains consisting of alternating face-sharing AO_6 trigonal prisms and BO_6 octahedra as seen in Fig. 1b. Because the AO_3–BO_3 chains are widely separated at a distance of about 5.5 Å by the A' cations, A'_3ABO_6-type compounds are expected to show the characteristics of a 1-D system. Actually it has been reported that many A'_3ABO_6-type compounds exhibit the typical magnetic properties of 1-D materials: Sr_3ZnIrO_6 shows 1-D Ising antiferromagnetism with $S = 1/2$ (5), Sr_3CuIrO_6 shows 1-D Heisenberg ferromagnetism with $S = 1/2$ (6), Sr_3CuPtO_6 shows 1-D Heisenberg antiferromagnetism with $S = 1/2$ (7), and $Sr_3CuPt_{0.5}Ir_{0.5}O_6$ shows random spin chain paramagnetism (8).

The structure of A'_3ABO_6-type compounds has not only 1-D features but also 2-D features. Figure 2 shows the structure of A'_3ABO_6-type compounds projected on the c-plane. Each AO_3–BO_3 chain is surrounded by six parallel neighboring chains, forming a triangular lattice in the basal plane. Therefore, this system can be also regarded as a triangular lattice system and can be expected to show peculiar behavior originating from geometrical frustration if the interchain interactions are antiferromagnetic. For example, $Ca_3Co_2O_6$ exhibits the magnetic properties characteristic of a triangular spin lattice (9).

It is remarkable that A'_3ABO_6-type compounds have "unique 1-D chains." The structure of A'_3ABO_6-type compounds containing 1-D chains consists of alternating two different spins in A and B sites, although the structures of $CuGeO_3$ and Y_2BaNiO_5 contain 1-D chains consisting of identical spins. Namely, A'_3ABO_6-type compounds are alternating spin systems. Because of many combinations of A and B sites, there can be various systems with two different alternating spins. Recently, interesting results were predicted from the theoretical investigation on the quantum behavior of mixed-spin chains with two kinds of spins (10). Therefore, one can expect that this alternating spin system shows new magnetic properties.

We have reported the synthesis and characterization of new A'_3ABO_6-type compounds, Ca_3CoIrO_6 and Ca_3CoRuO_6 (11). Ca_3CoIrO_6 exhibits the complex magnetic behavior. In this compound, the characteristic field dependence of the magnetization was observed at the temperature ranging from 80 to 32 K with decreasing

[1] To whom correspondence should be addressed.

0022-4596/99 $30.00

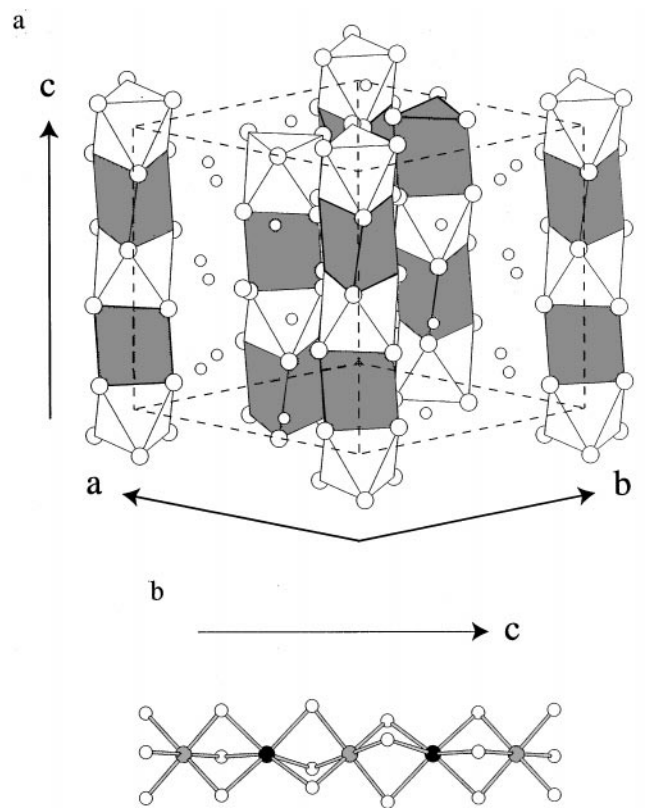

FIG. 1. (a) The structure of A'_3ABO_6-type compounds. The open and shaded polyhedra represent BO_6 octahedra (antitrigonal prisms) and AO_6 trigonal prisms, respectively. The large and small open circles represent the oxygen and A' atoms, respectively. (b) A single chain consisting of alternating AO_6 trigonal prisms and BO_6 octahedra. The solid circles stand for A atoms, the shaded circles B atoms, and the open circles for oxygen.

temperature, which is caused by the development of the short-range ferromagnetic order. Moreover, this compound showed a steep decrease in the magnetization at 32 K. It has been suggested that the ground state in this compound is a canted antiferromagnetic state. This behavior has also been seen in Sr_3NiIrO_6 (6). On the contrary, Ca_3CoRuO_6 orders antiferromagnetically with $T_N = 55$ K without any anomalous behavior.

Recently, we have succeeded in synthesizing new A'_3ABO_6-type compounds, Ca_3CoRhO_6 and Ca_3FeRhO_6. In this paper, we report the syntheses, structural characterizations, and magnetic properties of these compounds. The structure of Ca_3CoRhO_6 and Ca_3FeRhO_6 contains 1-D chains consisting of alternating face-sharing CoO_6/FeO_6 trigonal prisms and RhO_6 octahedra, respectively. Ca_3CoRhO_6 exhibits magnetic behavior similar to Sr_3NiIrO_6 and Ca_3CoIrO_6. In the case of Ca_3FeRhO_6, a sharp cusp is observed in the magnetic susceptibility at 12 K.

2. EXPERIMENT

Polycrystalline samples of Ca_3CoRhO_6 and Ca_3FeRhO_6 were prepared by solid state reaction. Stoichiometric amounts of $CaCO_3$ (99.99%), CoO (99.99%), Fe_2O_3 (99.99%), and Rh (> 99.95%) were mixed using an agate mortar and pestle and pressed into pellets. The pellets were placed on an alumina boat and calcined at 1173 K for one day mainly to decompose the carbonate. Subsequently, the samples were heated in air for 1 or 2 weeks at 1473 K for Ca_3CoRhO_6 and at 1523 K for Ca_3FeRhO_6 with intermediate grindings.

Powder X-ray diffraction (XRD) measurements were performed at room temperatures using M18XHF22 (MAC Science Co., Ltd.) using Cu$K\alpha$ radiation, $\lambda = 1.5404$ Å, in the 2θ range of 10°–120° (Bragg Brentano geometry). A scan step of 0.02° and a recording time of 1 sec was applied for each step. Five step scans were collected and summed for Rietveld analysis. The Rietveld analysis (12) of the powder XRD data were performed using the refinement package Rietan (13).

Magnetic susceptibility $\chi(=M/H)$ was measured by a superconducting quantum interference device (SQUID) magnetometer. Magnetic data were obtained in various applied fields in the temperature range 2–330 K after cooling the sample in zero magnetic field (zero-field cooled,

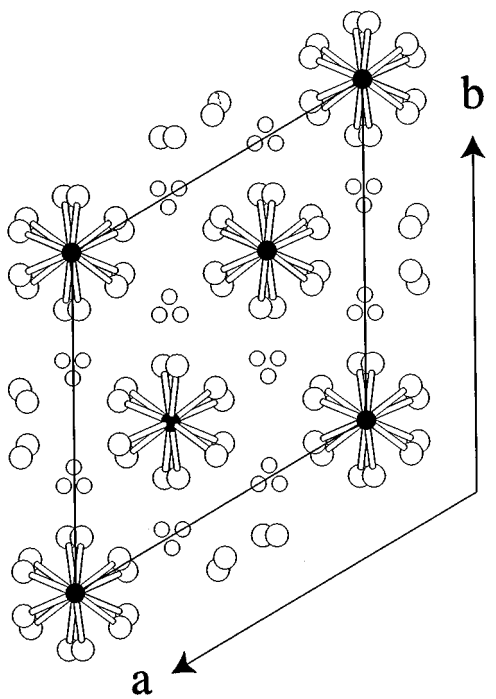

FIG. 2. The structure view projected to the basal plane. The solid circles represent A and B atoms, the large open circles the oxygen, and the small open circles A' atoms.

ZFC) and also after cooling in the measured field (field cooled, FC).

3. RESULTS AND DISCUSSION

3.1. Crystal Structure of Ca_3CoRhO_6

The powder XRD pattern of Ca_3CoRhO_6 is shown in Fig. 3. Although three extra peaks at the 2θ angles $\sim 18°$, $\sim 23°$, and $\sim 50°$ caused by unknown impurities were observed, their XRD intensities are very small compared with those of Ca_3CoRhO_6 so that they will not disturb any intrinsic magnetic properties of Ca_3CoRhO_6. The powder X-ray Rietveld refinement was carried out both with the space group $R\bar{3}c$ (No. 167) using the structure of Sr_3MgRhO_6 (14) and with the space group $C2/c$ (No. 15) using the structure of Sr_3CuPtO_6 (4) as the starting model. All attempts to refine the structure using the latter model were not successful. Refinement using the space group and atomic positions of Sr_3MgRhO_6 gave a unit cell of $a = 9.2017(1)$ Å, $c = 10.7296(1)$ Å and quickly converged to $R_{WP} = 12.41\%$, $R_P = 8.19\%$, $R_e = 3.20\%$. Although several attempts were made to refine the structural parameters by varying site occupancies, e.g., the deficiencies and/or the substitution in Rh site, these did not improve the result. The calculated pattern and the difference between observed and calculated one are also shown in Fig. 3. The refined structural parameters are summarised in Table 1. Observed and calculated interplanar spacing and intensity for each reflection are given in Table 2. Selected interatomic distances are presented in Table 3. The nearest neighbor interchain distance is 5.313 Å. Thus, the structure of Ca_3CoRhO_6 can be confirmed to contain 1-D chains consisting of alternating face-sharing CoO_6 trigonal prisms and RhO_6 octahedra.

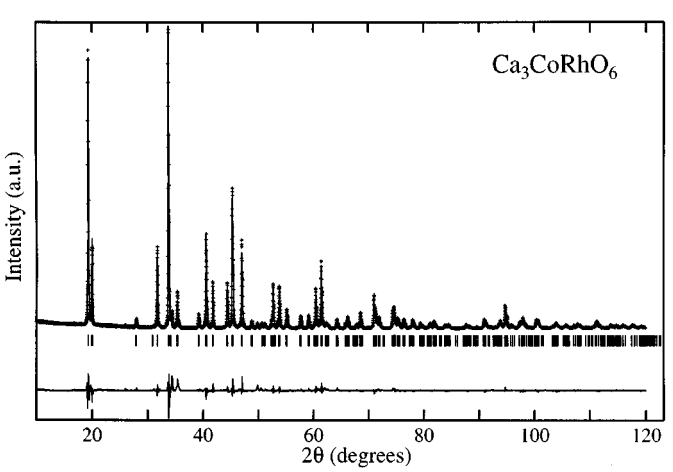

FIG. 3. Observed (dotted) and calculated (solid line) X-ray profile of Ca_3CoRhO_6. Tick marks indicate the positions of allowed Bragg reflections. The difference between observed and calculated values (observed value minus calculated one) is located at the bottom of the figure.

TABLE 1
Atomic Positions and Isothermal Parameters for Ca_3CoRhO_6 and Ca_3FeRhO_6

Compound	Atom	Site	x	y	z	B (Å)
Ca_3CoRhO_6	Ca	18e	0.3666(1)	0	0.25	0.20(3)
$a = 9.2017(1)$ Å	Co	6a	0	0	0.25	0.23(4)
$c = 10.7296(1)$ Å	Rh	6b	0	0	0	0.17(2)
	O	36f	0.1823(3)	0.0230(4)	0.1145(2)	0.53(7)
Ca_3FeRhO_6	Ca	18e	0.3677(3)	0	0.25	0.25(6)
$a = 9.1960(1)$ Å	Fe	6a	0	0	0.25	0.09(8)
$c = 10.7861(1)$ Å	Rh	6b	0	0	0	0.10(4)
	O	36f	0.1849(8)	0.0238(9)	0.1181(6)	0.97(18)

3.2. Crystal Structure of Ca_3FeRhO_6

The powder XRD pattern of Ca_3FeRhO_6 is shown in Fig. 4. $Ca_2Fe_2O_5$, which is an antiferromagnet with $T_N = 725$ K (15), was found as only a minor impurity phase as seen in Fig. 4. We assume that this is because a small amount of rhodium was volatilized as Rh_2O_3 or incorporated in an amorphous impurity phase (14). Since its XRD intensities are very small, it will have little effect on the observed magnetic data. For Ca_3FeRhO_6, the powder

TABLE 2
Observed and Calculated Powder XRD of Ca_3CoRhO_6 ($R\bar{3}c$, $a = 9.2017$ Å, $c = 10.7296$ Å)

hkl	d_{obs}	d_{cal}	I/I_0(obs)	I/I_0(cal)
110	4.5844	4.6009	84	84
012	4.4347	4.4503	23	30
202	3.1891	3.1987	2	2
113	2.8159	2.8237	26	28
300	2.6495	2.6563	100	100
122	2.6112	2.6264	5	3
104	2.5355	2.5422	10	11
220	2.2949	2.3004	5	5
024	2.2201	2.2251	31	40
131	2.1598	2.1647	17	15
312	2.0393	2.0436	17	17
214	1.9990	2.0032	50	59
223	1.9307	1.9348	33	32
042	1.8640	1.8676	3	3
321	1.8000	1.8022	1	1
006	1.7845	1.7883	2	2
125	1.7440	1.7477	3	3
410	1.7355	1.7390	15	16
232		1.7305		< 1
134	1.7027	1.7058	16	19
116	1.6639	1.6668	7	10
404	1.5966	1.5994	5	6
143	1.5613	1.5639	5	3
413		1.5639		2

TABLE 3
Selected Interatomic Distances (Å) of Ca_3CoRhO_6 and Ca_3FeRhO_6

Compound	Bond	Distance	Bond	Distance
Ca_3CoRhO_6	Co–O	2.149(5)	Co–Ca	3.373(1)
	Rh–O	2.003(5)	Rh–Ca	3.0598(4)
	Co–Rh	2.6824(1)		
Ca_3FeRhO_6	Fe–O	2.143(12)	Fe–Ca	3.381(2)
	Rh–O	2.047(12)	Rh–Ca	3.055(1)
	Fe–Rh	2.6965(1)		

TABLE 4
Observed and Calculated Powder XRD of Ca_3FeRhO_6 ($R\bar{3}c$, $a = 9.1960$ Å, $c = 10.7861$ Å)

hkl	d_{obs}	d_{cal}	I/I_0(obs)	I/I_0(cal)
110	4.5927	4.5980	75	82
012	4.4607	4.4655	23	27
202	3.1998	3.2034	2	2
113	2.8291	2.8323	24	29
300	2.6517	2.6547	100	100
122	2.6275	2.6284	3	3
104	2.5520	2.5541	11	11
220	2.2966	2.2990	5	5
024	2.2304	2.2328	37	42
131	2.1616	2.1639	18	16
312	2.0420	2.0440	18	17
214	2.0063	2.0085	57	59
223	1.9350	1.9369	27	29
042	1.8659	1.8678	3	3
321	1.7998	1.8014	2	1
006	1.7952	1.7977	1	2
125	1.7517	1.7534	4	4
410	1.7363	1.7379	16	17
232		1.7305		< 1
134	1.7072	1.7087	18	20
116	1.6728	1.6743	8	10
404	1.6003	1.6017	5	5
143	1.5632	1.5647	4	4
413		1.5647		2

X-ray two-phase Rietveld refinement was carried out both with the space group $R\bar{3}c$ (No. 167) using the structure of Sr_3MgRhO_6 (14) and with the space group $C2/c$ (No. 15) using the structure of Sr_3CuPtO_6 (4) as the starting model of Ca_3FeRhO_6. As the structural parameters of $Ca_2Fe_2O_5$, the structural data reported by Colville (16) were used. All attempts to refine the structure in the space group $C2/c$ were not successful. Refinement using the space group $R\bar{3}c$ (No. 167) gave a unit cell of $a = 9.1960(1)$ Å, $c = 10.7861(1)$ Å and successfully converged to $R_{WP} = 13.27\%$, $R_P = 8.70\%$, $R_e = 2.98\%$. Although several attempts were made to refine the structural parameters by varying site occupancies similar to the structural refinement for Ca_3CoRhO_6, these did not improve the result. The calculated pattern and the difference between the observed and the calculated one are also shown in Fig. 4. The refined structural parameters are summarised in Table 1. Observed and calculated interplanar spacing and intensity for each reflection are given in Table 4. Selected interatomic distances are also presented in Table 3. The interchain distance is 5.309 Å. The structure of Ca_3FeRhO_6 contains 1-D chains consisting of alternating face-sharing FeO_6 trigonal prisms and RhO_6 octahedra.

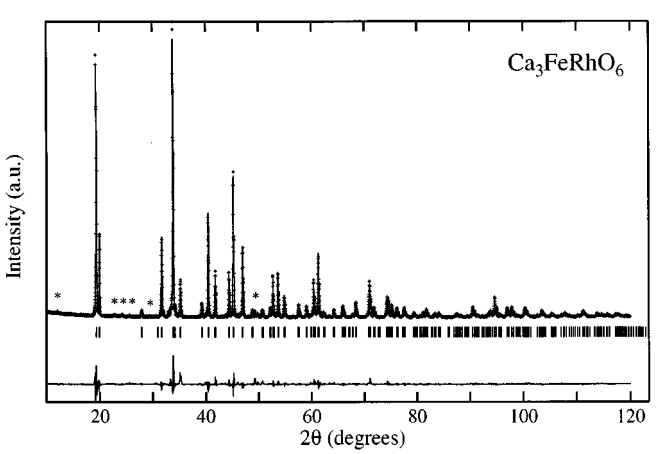

FIG. 4. Observed (dotted) and calculated (solid line) X-ray profile of Ca_3FeRhO_6. Tick marks indicate the positions of allowed Bragg reflections. The difference line, observed minus calculated, is located at the bottom of the figure. The peaks attached by asterisk marks correspond to $Ca_2Fe_2O_5$.

3.3. *Magnetic Properties of Ca_3CoRhO_6*

The temperature dependences of the magnetizations of Ca_3CoRhO_6 measured at $H = 1$, 10, 30, and 50 kOe are shown in Fig. 5. It is characteristic that there is a sharp drop at $T_c \sim 35$ K in the magnetizations for ZFC. For FC, the magnetizations do not show any such sharp drops, approaching the constant values which depend on the applied field.

The temperature dependences of the magnetic susceptibilities M/H of Ca_3CoRhO_6 measured at $H = 1$, 10, 30, and 50 kOe are shown in Fig. 6. The susceptibility shows Curie–Weiss-like behavior from 220 to 330 K. The Curie constant C_{exp} and the Weiss temperature θ estimated from the susceptibility data are 2.47 emu/(mol·K) and 150.0 K. The ideal value of Curie constant, C_{ideal}, can be calculated for all possible cases from ion valences and spin states based on two conditions of the g factor with 2 and low spin state in Rh ions. Assuming that the Co ions are in the divalent state with $S_A = 3/2$ (high spin state) and the Rh ions in the tetravalent state with $S_B = 1/2$ (low spin state), the obtained

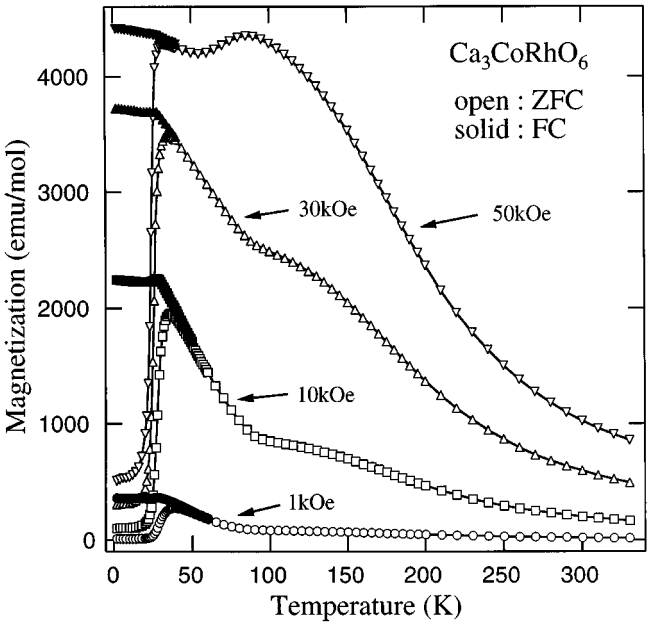

FIG. 5. The temperature dependences of the magnetization of Ca_3CoRhO_6 measured at $H = 1$, 10, 30, and 50 kOe. Open symbols stand for ZFC and solid symbols for FC.

value of C_{ideal} is found to be 2.25 emu/(mol·K), very close to C_{exp}. Here, S_A and S_B stand for the quantum spin number of the A and B sites, respectively. The second possible value $C_{ideal} = 3.00$ emu/(mol·K) for the Co ions in the trivalent state with $S_A = 2$ (high spin state) and the Rh ions in the trivalent state with $S_B = 0$ (low spin state) deviates largely from C_{exp}. Bond valence calculation was carried out using the data in Table 3. The bond valence sum of Rh cannot be calculated because no parameter is available for Rh^{4+} (14). Using a tabulated parameter (17), the estimated valence of Co is 1.74, close to the valence of Co estimated from the susceptibility data. It can, therefore, be considered that Ca_3CoRhO_6 contains 1-D chains consisting of alternating Co^{2+} with $S_A = 3/2$ spin and Rh^{4+} with $S_B = 1/2$ spin. We can also consider that the positive value θ implies the ferromagnetic exchange interaction between spins. One can note the deviation from the Curie–Weiss law below 220 K. The values of M/H depend on H for $T \leq 90$ K. The susceptibility at 1 kOe increases steeply. The enhancement of M/H at 90 K is damped with increasing H. The susceptibility at 50 kOe is almost constant down to 35 K. The increase of the susceptibilities suggests the development of the ferromagnetic short-range order, which agrees with the positive Weiss temperature. The susceptibilities for ZFC measurement sharply drop at $T_c \sim 35$ K into the constant low value which is independent of H. The susceptibilities for FC measurement show no drop and is close to relatively large constant values which are dependent on H.

The magnetic behavior of Ca_3CoRhO_6 is similar to those of Sr_3NiIrO_6 (6) and Ca_3CoIrO_6 (11) as follows: (1) the susceptibilities obey the Curie–Weiss law at high temperatures, (2) there is a deviation from the Curie–Weiss law at $T < 150$ K, (3) the values of M/H depend on H below 70 K for Sr_3NiIrO_6 and below 80 K for Ca_3CoIrO_6, and (4) there is an abrupt drop at $T_c = 21$ K for Sr_3NiIrO_6 and at $T_c = 32$ K for Ca_3CoIrO_6. Consequently, it is considered that these three compounds have similar magnetic properties. Nguyen *et al.*, reported that the Ni ions in Sr_3NiIrO_6 are in the divalent state with $S_A = 1$ and the Ir ions are in the tetravalent state with $S_B = 1/2$. Namely, Sr_3NiIrO_6 contains 1-D chains consisting of alternating Ni^{2+} with $S_A = 1$ spin and Ir^{4+} with $S_B = 1/2$ spin. It is interesting that Ca_3CoRhO_6 and Ca_3CoIrO_6 with $S_A = 3/2$, $S_B = 1/2$ indicate a magnetic behavior similar to that of Sr_3NiIrO_6 with $S_A = 1$, $S_B = 1/2$.

The field dependence of the magnetizations measured at several temperatures are shown in Fig. 7. The magnetization curves at 2 and 20 K, where the susceptibilities have the low values which are independent of H as seen in Fig. 6, show little increase and the values of the magnetizations at 50 kOe are very small compared with 5585 emu/mol ($= 1\ \mu_B$/formula unit). Small hystereses are seen in the magnetization curves at 2 and 20 K. The magnetization curve at 25 K, however, exhibits relatively large hysteresis. The value of the magnetization at 50 kOe for 25 K is 6.6 times as large

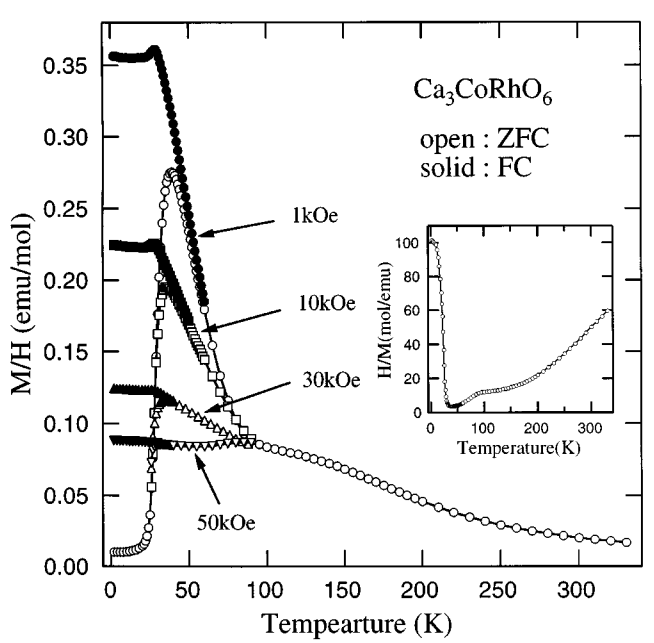

FIG. 6. The temperature dependences of the magnetic susceptibilities M/H of Ca_3CoRhO_6 measured at $H = 1$, 10, 30, and 50 kOe. Open symbols represent ZFC and solid symbols represent FC. The inverse magnetic susceptibility H/M measured at $H = 1$ kOe for ZFC measurement is shown in the inset.

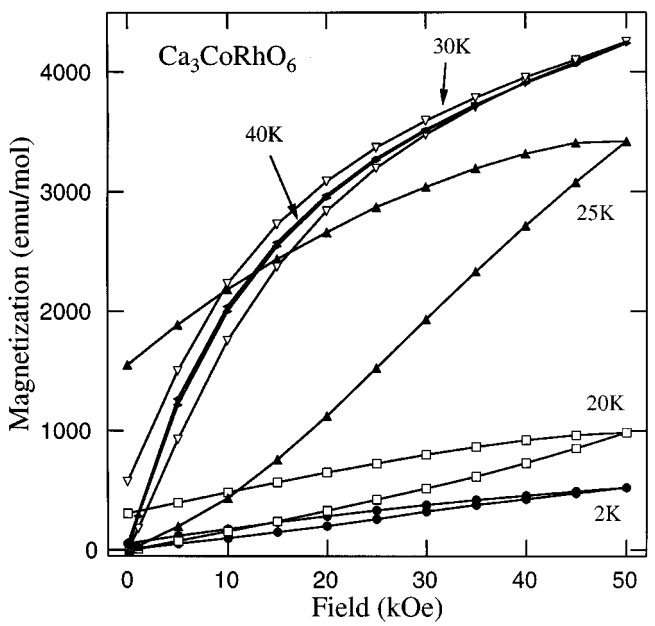

FIG. 7. The field dependence of the magnetizations of Ca_3CoRhO_6 measured at several temperatures.

as that at 50 kOe for 2 K. At the temperature 25 K, the susceptibilities are dropping into the constant small value as seen in Fig. 6. The magnetization curves at 30 and 40 K are typical of an ordinary soft ferromagnet. There still exists small hysteresis in the magnetization curve at 40 K.

We, here, discuss qualitatively the magnetic properties of Ca_3CoRhO_6. The positive Weiss temperature $\theta = 150$ K suggests that the intrachain exchange interaction is ferromagnetic, taking into consideration that the intrachain distance between neighboring Co and Rh ions is about half as long as the interchain distance. In light of the ferromagnetic intrachain interaction, we can consider that the steep increases at $T = 90$ K in the susceptibilities is due to the development of the ferromagnetic short-range order of spins within a chain. At $T_c \sim 35$ K there is a precipitous drop in the susceptibilities for ZFC measurement, suggesting that the interchain interactions is antiferromagnetic. Since there is the large difference between ZFC and FC in the susceptibilities below T_c, the ground state of Ca_3CoRhO_6 is not considered to be a spin singlet state. The neutron diffraction studies at 10 K in Sr_3NiIrO_6 which has a magnetic property similar to Ca_3CoRhO_6 indicated that no structural change was observed with the exception of the thermal contraction in the unit cell parameters and that no additional peak according to the existence of a magnetic superstructure was observed (6). Taking these neutron experiments into account, we suppose that the ground state of Ca_3CoRhO_6 is a spin-freezing state. Since the CoO_3–RhO_3 chains in Ca_3CoRhO_6 form a triangular lattice, the spin frustrations characteristic to a triangular lattice are expected due to the antiferromagnetic interchain interaction. Therefore, the ground state of Ca_3CoRhO_6 is supposed to be a spin-freezing state which is caused by the competition with the antiferromagnetic interchain interactions. Further study is needed in order to confirm the ground state of Ca_3CoRhO_6 being a spin-freezing state.

3.4. *Magnetic Properties of Ca_3FeRhO_6*

In Fig. 8 is shown the temperature dependence of the magnetic susceptibility χ of Ca_3FeRhO_6 measured at $H = 1$ kOe. The χ shows Curie–Weiss-like behavior in the temperature range from 22 to 330 K. There was observed no difference between ZFC and FC in the susceptibility ranging from 2 to 330 K. The Curie constant C_{exp} and the Weiss temperature θ calculated from the susceptibility data are 3.38 emu/(mol·K) and -15.7 K. The value of Curie constant C_{ideal} can be obtained in the same way as Ca_3CoRhO_6 assuming that the g factor is 2 and Rh ions are in low spin state. If the Fe ions are divalent with $S_A = 2$ (high spin state) and the Rh ions tetravalent with $S_B = 1/2$ (low spin state), the obtained Curie constant C_{ideal} is 3.38 emu/(mol·K), coincident with C_{exp}. The second possible value of C_{ideal} is 4.38 emu/(mol·K) for the Fe ions in the trivalent state with $S_A = 5/2$ (high spin state) and the Rh ions in the trivalent state with $S_B = 0$ (low spin state) and deviates largely from C_{exp}. The bond valence sum of Fe calculated from the data in Table 3 is 1.99, close to the valence of Fe estimated from

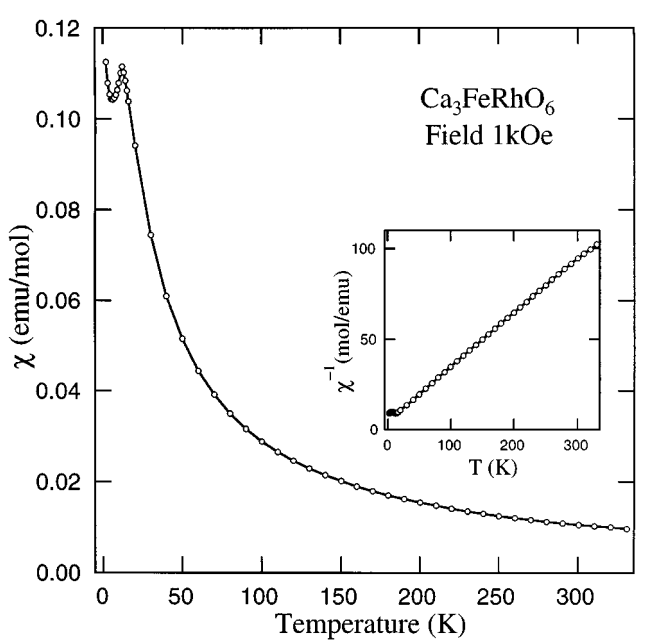

FIG. 8. The temperature dependence of the magnetic susceptibility of Ca_3FeRhO_6 measured at 1 kOe. The inverse susceptibility is shown in the inset as a function of temperature.

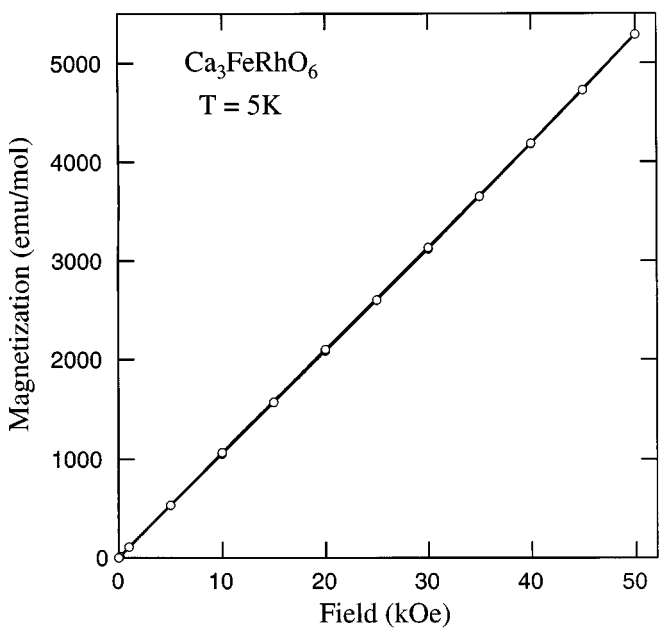

FIG. 9. The field dependence of the magnetization of Ca_3FeRhO_6 measured at 5 K.

the susceptibility data. Therefore, Ca_3FeRhO_6 contains 1-D chains consisting of alternating Fe^{2+} with $S_A = 2$ spin and Rh^{4+} with $S_B = 1/2$ spin. The maximum observed at 12 K in Fig. 8 indicates the presence of antiferromagnetic interaction, which agrees with the negative value of θ. The increase in the susceptibility below 6 K is presumably due to paramagnetic impurities. It is likely that the maximum at 12 K shows an ordinary three-dimensional antiferromagnetic transition because of the acute shape of the maximum, though we can possibly regard it as the short range ordering of the 1-D antiferromagnetic chain. The field dependence of the magnetization of Ca_3CoRhO_6 measured at 5 K is shown in Fig. 9. A linear relation between the magnetization and magnetic field was observed for Ca_3CoRhO_6 at $0 \leq H \leq 50$ kOe.

4. CONCLUSION

We have synthesized and characterized the structure and measured magnetic properties of 1-D A'_3ABO_6-type compounds, Ca_3CoRhO_6 and Ca_3FeRhO_6. Ca_3CoRhO_6 and Ca_3FeRhO_6 contain the 1-D chains consisting of alternating face-sharing CoO_6, FeO_6 trigonal prisms and RhO_6 octahedra, respectively. The susceptibilities of Ca_3CoRhO_6 show the steep drop at $T_c \sim 35$ K for ZFC whereas they show constant large values for FC, suggesting the antiferromagnetic interchain exchange-coupling of ferromagnetic chains. The magnetic behavior of Ca_3CoRhO_6 is similar to those of Sr_3NiIrO_6 and Ca_3CoIrO_6. It is considered that these three compounds have similar magnetic properties, although their detailed magnetic structure is unknown. Further study is needed for full understanding. Ca_3FeRhO_6 exhibits the three-dimensional antiferromagnetic transition at 12 K.

ACKNOWLEDGMENT

This work was partly supported by a Grant-in-Aid for Scientific Research from the Ministry of Education, Science and Culture (09440241, 10740323).

REFERENCES

1. M. Hase, I. Terasaki, and K. Uchinokura, *Phys. Rev. Lett.* **70,** 3651 (1993).
2. J. Darriet and L. P. Regnault, *Solid State Commun.* **86,** 409 (1993).
3. M. Mekata and K. Adachi, *J. Phys. Soc. Jpn.* **44,** 806 (1978).
4. A. P. Wilkinson, A. K. Cheetham, W. Kunnman, and Å. Kvick, *Eur. J. Solid State Inorg. Chem.* **28,** 453 (1991).
5. C. Lampe-Önnerud, M. Sigrist, and H.-C. zur Loye, *J. Solid State Chem.* **127,** 25 (1996).
6. T. N. Nguyen and H.-C. zur Loye, *J. Solid State Chem.* **117,** 300 (1995).
7. T. N. Nguyen, D. M. Giaquinta, and H.-C. zur Loye, *Chem. Mater.* **6,** 1642 (1994).
8. T. N. Nguyen, P. A. Lee, and H.-C. zur Loye, *Science* **271,** 489 (1996).
9. H. Kageyama, K. Yoshimura, K. Kosuge, H. Mitamura, and T. Goto, *J. Phys. Soc. Jpn.* **66,** 1607 (1997).
10. S. Yamamoto and T. Fukui, *Phys. Rev. B* **57,** 14008 (1998).
11. H. Kageyama, K. Yoshimura, and K. Kosuge, *J. Solid State Chem.* **140,** 14 (1998).
12. H. M. Rietveld, *J. Appl. Crystallogr.* **2,** 65 (1969).
13. F. Izumi, *in* "The Rietveld Method" (R. A. Young, Ed.), Chap. 13. Oxford University Press, Oxford, 1993; Y.-I. Kim and F. Izumi, *J. Ceram. Soc. Jpn.* **102,** 401 (1994).
14. P. Núñez, S. Trail, and H.-C. zur Loye, *J. Solid State Chem.* **130,** 35 (1997).
15. P. Marchukov, R. Geick, C. Brotzeller, W. Treutmann, E. G. Rudashevsky, and A. M. Balbashov, *Phys. Rev. B* **48,** 13538 (1993).
16. A. A. Colville, *Acta Crystallogr. B* **26,** 1469 (1970).
17. N. E. Bresse and M. O'Keeffee, *Acta Crystallogr. B* **47,** 192 (1991).